Electric dipole moments in the minimal scotogenic model

Asmaa Abada[a] **and Takashi Toma**[b]

[a]*Laboratoire de Physique Théorique, CNRS, Univ. Paris-Sud, Université Paris-Saclay, 91405 Orsay, France*

[b]*Physik-Department T30d, Technische Universität München, James-Franck-Straße, D-85748 Garching, Germany*

E-mail: asmaa.abada@th.u-psud.fr, takashi.toma@tum.de

ABSTRACT: In this work we consider a minimal version of the scotogenic model capable of accounting for an electron electric dipole moment within experimental sensitivity reach in addition to providing a dark matter candidate and radiatively generating neutrino masses. The Standard Model is minimally extended by two sterile fermions and one inert scalar doublet, both having odd parity, while the Standard Model particles have an even parity, imposed by a $\mathbb{Z}_2$ symmetry. The neutrino Yukawa couplings provide additional sources of CP violation, and thus a possible impact on electric dipole moments of charged leptons. This model provides two possible dark matter candidates (one bosonic and one fermionic) and our results show that, independently of the ordering of the generated light neutrino spectrum, one can have sizeable electron electric dipole moment within ACME sensitivity reach in the case of fermionic dark matter candidate.

Contents

1 Introduction

Although the Standard Model (SM) provides a successful description of physics below the electroweak scale, it cannot accommodate the tiny neutrino masses suggested by neutrino oscillation experiments. One of the simplest options to generate non-zero neutrino masses at tree level is the seesaw mechanism, such as the Type-I [1–5], Type-II [6, 7], Type-III [8], inverse [9] and linear seesaw mechanisms [10, 11].

On the other hand, exploring CP violation is important since it is one of the necessary ingredients at the origin of the baryon asymmetry of the Universe (BAU). Although CP violation in the SM has been confirmed in the quark sector, it is not large enough to reproduce the BAU as observed by the Planck Collaboration, $n_s/s = (8.59 \pm 0.11) \times 10^{-11}$ [12]. The possibility of CP violation in the lepton sector fueled the interest of generating the BAU via leptogenesis, as proposed in ref. [13], where a lepton asymmetry arises from lepton number and CP violating out-of-equilibrium decays of (heavy) right-handed neutrinos. In addition, neutrinoless double beta decay ($0\nu2\beta$) is the observable associated with the

existence of Majorana neutrinos and with CP violating phases; many other processes reflecting total lepton number violation by two units ($\Delta L = 2$), as in the case of the latter observable, are being actively searched for. For instance, at colliders, there are several possible signatures of lepton number violation [14–20]. As pointed out in several analyses, neutrino Majorana phases can also give rise to non-vanishing contributions to charged lepton electric dipole moments (EDMs) [21]; in particular, the computation of EDMs in the presence of right-handed neutrinos (like in the Type-I seesaw model) has been addressed in refs. [22–24].

Recently, working in the framework of a "$3 + n_S$" (SM extended by a number n_S of sterile fermions) model, a derivation of the 2-loop analytical expressions allowed to show that a non-vanishing contribution to the EDMs requires at least the addition of two non-degenerate sterile states to the SM field content [25]. A numerical evaluation of the contributions to the charged lepton EDMs in the case of the simple "3+2" toy model showed that, provided the masses of the two mostly sterile states are in the range from 100 GeV to 100 TeV, it is possible to have $|d_e|/e \geq 10^{-30}$ cm (although for the muon and tau EDMs the predictions remain several orders of magnitude below the corresponding future sensitivities) [25]. Interestingly, part of the regimes leading to sizable electron EDM within ACME next generation [26, 27] reach are also within detection reach of a future ILC. This is in contrast with the inverse seesaw realization, where minimal realizations have been found in ref. [28], and for which it was shown in ref. [29] that charged lepton EDMs can indeed be enhanced by large neutrino Yukawa couplings, naturally present in the inverse seesaw models. However, the maximum value of the predicted electron EDM is $|d_e^{\max}|/e \sim 5 \times 10^{-31}$ cm, lying two orders of magnitude below the current experimental bound, $|d_e|/e \leq 8.7 \times 10^{-29}$ cm, and thus marginally short of the future sensitivity, $|d_e|/e \sim 10^{-30}$ cm [26, 27].

The computation of charged lepton EDMs that has been done in the context of tree level seesaw mechanisms can straightforwardly be applied to the framework of radiative seesaw models, where small neutrino masses are generated at (one) loop level. Many models with radiative neutrino masses have been proposed so far. One interesting feature of the framework we consider in this study is that a dark matter candidate is also naturally included due to an imposed symmetry which forbids the Dirac neutrino mass term at tree level, and also stabilizes a lightest new particle, rendering it a possible dark matter candidate. The scotogenic model which has been proposed by Ma [30] is the simplest model with radiative neutrino masses, and is well-studied as a benchmark model. In this model, the new Yukawa couplings between leptons and the new particles play an important role in generating neutrino masses at the one-loop level and in providing an interactive dark matter.

In this work, we explore the effect and the magnitude of CP violation in the scotogenic model by computing the electron EDM while taking into account all experimental and theoretical constraints such as lepton flavour violation, electroweak precision data, dark matter searches, vacuum stability and the perturbativity of the couplings.

The paper is organised as follows: in section 2 we present the basic set up of the minimal scotogenic model we consider, the derivation of neutrino masses and the parametrization we adopt. In section 3, we give the detailed computation of the electron EDM. We collect

the relevant experimental and theoretical constraints that we impose in our analysis in section 4. The numerical results are presented in section 5, and our final remarks and discussion are collected in section 6. In the appendix, we give the general formulae of the loop functions for the charged lepton EDMs in the scotogenic model.

2　The model

In the original version of the scotogenic model, which has been proposed in ref. [30], the SM was extended by three singlet fermions N_i $(i = 1, 2, 3)$ and one inert scalar doublet η. In this work, we consider the same model but with only two massive neutral (sterile) fermions N_i $(i = 1, 2)$ with the aim of minimising the degrees of freedom; in this case, only two non-zero (light) neutrino mass eigenvalues can be generated at one-loop level, the lightest neutrino remaining massless. A $\mathbb{Z}_2$ symmetry is imposed such that the new particles have odd parity, while the SM particles have even parity. The Lagrangian involving the new particles is given by

$$\mathcal{L} = (D_\mu \eta)^\dagger (D^\mu \eta) + \frac{1}{2} \overline{N_i} \left(i \slashed{\partial} - m_i \right) N_i - y_{i\alpha} \eta \overline{N_i} P_L L_\alpha + \text{H.c.} , \tag{2.1}$$

where L_α $(\alpha = e, \mu, \tau)$ are the SM left-handed lepton doublets and where m_i $(i = 1, 2)$ denotes the mass of the sterile fermions taking $m_1 < m_2$. With the additional inert scalar doublet η, the scalar potential $\mathcal{V}$ becomes

$$\mathcal{V} = \mu_H^2 |H|^2 + \mu_\eta^2 |\eta|^2 + \frac{\lambda_1}{2} |H|^4 + \frac{\lambda_2}{2} |\eta|^4 + \lambda_3 |H|^2 |\eta|^2 + \lambda_4 |\eta^\dagger H|^2 + \frac{\lambda_5}{2} \left[\left(\eta^\dagger H \right)^2 + \text{H.c.} \right]. \tag{2.2}$$

The coupling λ_5 is generally complex, however the CP phase can be absorbed by a field redefinition of the doublet scalar η. Thus one can always consider $\lambda_5 > 0$, putting the new CP violating phases in the Yukawa coupling $y_{i\alpha}$ of eq. (2.1). After the electroweak symmetry breaking, the neutral component of the inert scalar, $\eta^0 = (\eta_R + i\eta_I)/\sqrt{2}$, splits into the CP-even state η_R and the CP-odd one η_I, whose masses are respectively given by

$$m_R^2 = \mu_\eta^2 + (\lambda_3 + \lambda_4 + \lambda_5) \langle H \rangle^2 , \tag{2.3}$$

$$m_I^2 = \mu_\eta^2 + (\lambda_3 + \lambda_4 - \lambda_5) \langle H \rangle^2 , \tag{2.4}$$

where $\langle H \rangle$ is the vacuum expectation value of the SM Higgs boson H. Notice that one can deduce from eqs. (2.3), (2.4) that the latter squared mass difference is given by

$$m_R^2 - m_I^2 = 2\lambda_5 \langle H \rangle^2 . \tag{2.5}$$

As will be explained later, we focus on the case where the CP-even and CP-odd states are nearly degenerate ($m_R \approx m_I$) in order to have large enough Yukawa couplings $y_{i\alpha}$ to generate sizeable electron EDM. The mass of the charged scalar η^+ and the average of the squared mass of CP-even and CP-odd states are given by

$$m_{\eta^+}^2 = \mu_\eta^2 + \lambda_3 \langle H \rangle^2 , \quad m_{\eta^0}^2 = (m_R^2 + m_I^2)/2 . \tag{2.6}$$

– 3 –
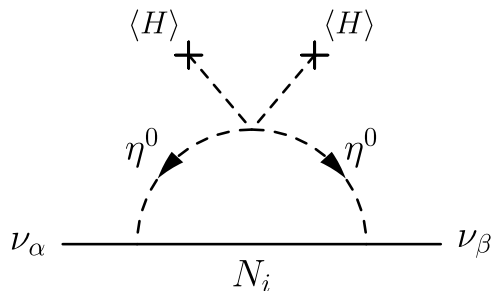
Figure 1. Diagram for Majorana neutrino masses at one-loop level.

In this model, Majorana neutrino masses for left-handed neutrinos are induced at one-loop level as shown in figure 1 and the (3×3) neutrino mass matrix is computed as

$$(m_\nu)_{\alpha\beta} = \sum_{i=1}^{2} \frac{y_{i\alpha} y_{i\beta} m_i}{2(4\pi)^2} \left[\frac{m_R^2}{m_R^2 - m_i^2} \log\left(\frac{m_R^2}{m_i^2}\right) - \frac{m_I^2}{m_I^2 - m_i^2} \log\left(\frac{m_I^2}{m_i^2}\right) \right] . \tag{2.7}$$

In the particular case where the mass splitting between m_R and m_I is small (i.e. when the coupling λ_5 is small, see eq. (2.5)), the Majorana neutrino mass matrix is simplified as

$$(m_\nu)_{\alpha\beta} \approx \sum_{i=1}^{2} \frac{y_{i\alpha} y_{i\beta} m_i}{(4\pi)^2} \frac{\lambda_5 \langle H \rangle^2}{m_{\eta^0}^2 - m_i^2} \left[1 - \frac{m_i^2}{m_{\eta^0}^2 - m_i^2} \log\left(\frac{m_{\eta^0}^2}{m_i^2}\right) \right] , \tag{2.8}$$

that we can parametrize as follows

$$(m_\nu)_{\alpha\beta} \equiv \left(y^T \Lambda \, y \right)_{\alpha\beta} , \tag{2.9}$$

where the (2×3) matrix y collects the Yukawa couplings $y_{1\alpha}$ (first line) and $y_{2\alpha}$ (second line) with $\alpha = e, \mu, \tau$, and where the matrix Λ is given by

$$\Lambda = \begin{pmatrix} \Lambda_1 & 0 \\ 0 & \Lambda_2 \end{pmatrix}, \quad \text{with} \quad \Lambda_i = \frac{m_i}{(4\pi)^2} \frac{\lambda_5 \langle H \rangle^2}{m_{\eta^0}^2 - m_i^2} \left[1 - \frac{m_i^2}{m_{\eta^0}^2 - m_i^2} \log\left(\frac{m_{\eta^0}^2}{m_i^2}\right) \right] . \tag{2.10}$$

Interestingly, since the Majorana mass matrix is proportional to the coupling λ_5, the latter is directly linked to lepton number violation and thus, taking small λ_5 would be natural in the sense of t'Hooft [31] to induce small Majorana masses for the left-handed neutrinos.

The 3×3 neutrino mass matrix is diagonalized as $U_{\text{PMNS}}^T m_\nu U_{\text{PMNS}} = \text{diag}(\hat{m}_1, \hat{m}_2, \hat{m}_3)$ with the Pontecorvo-Maki-Nakagawa-Sakata (PMNS) matrix U_{PMNS} where $\hat{m}_1 = 0$ ($\hat{m}_3 = 0$) in the case of normal (inverted) ordering of the light neutrino spectrum. In this case, the PMNS matrix is parametrized as usual by

$$U_{\text{PMNS}} = \begin{pmatrix} 1 & 0 & 0 \\ 0 & \cos\theta_{23} & \sin\theta_{23} \\ 0 & -\sin\theta_{23} & \cos\theta_{23} \end{pmatrix} \begin{pmatrix} \cos\theta_{13} & 0 & e^{-i\delta_{\text{CP}}}\sin\theta_{13} \\ 0 & 1 & 0 \\ -e^{i\delta_{\text{CP}}}\sin\theta_{13} & 0 & \cos\theta_{13} \end{pmatrix}$$
$$\times \begin{pmatrix} \cos\theta_{12} & \sin\theta_{12} & 0 \\ -\sin\theta_{12} & \cos\theta_{12} & 0 \\ 0 & 0 & 1 \end{pmatrix} \begin{pmatrix} 1 & 0 & 0 \\ 0 & e^{i\varphi_{\text{CP}}} & 0 \\ 0 & 0 & 1 \end{pmatrix} . \tag{2.11}$$

The PMNS matrix includes one Dirac phase $\delta_{\rm CP}$ and one Majorana phase $\varphi_{\rm CP}$.[1] The 2×3 Yukawa matrix y defined in eq. (2.9) can be expressed adapting the Casas-Ibarra parametrization as [32]

$$y = \sqrt{\Lambda}^{-1} C \sqrt{\hat{m_\nu}} U_{\rm PMNS}^\dagger \,, \tag{2.12}$$

where C is a 2×3 matrix satisfying $CC^T = \mathbb{1}_{2\times 2}$. Furthermore, this matrix C can be parametrized as

$$C = \begin{pmatrix} 0 & \cos\xi & -\sin\xi \\ 0 & \kappa\sin\xi & \kappa\cos\xi \end{pmatrix}, \quad \text{for} \quad \text{normal hierarchy}\,, \tag{2.13}$$

$$C = \begin{pmatrix} \cos\xi & -\sin\xi & 0 \\ \kappa\sin\xi & \kappa\cos\xi & 0 \end{pmatrix}, \quad \text{for} \quad \text{inverted hierarchy}\,, \tag{2.14}$$

where κ is the sign parameter $\kappa = \pm 1$ and ξ is a complex angle. The non-zero 2×2 part of eq. (2.13) and (2.14) corresponds to an element of the $O(2, \mathbb{C})$ group, whose determinant is given by the parameter κ. Consequently, the 2×3 Yukawa matrix y can be defined in terms of 5 parameters experimentally determined by neutrino oscillation experiments (i.e. $\Delta\hat{m}_{ij}^2$ and the three mixing angles) and 7 free parameters that are: Λ_1, Λ_2, $\delta_{\rm CP}$, $\varphi_{\rm CP}$ and the matrix C which includes three free real parameters. Hereafter we express $\sin\xi$ as $\sin\xi = |\sin\xi|e^{i\eta_{\rm CP}}$.

Since the lightest $\mathbb{Z}_2$ odd particle is stabilized, the model also includes a dark matter candidate which, depending on the mass hierarchy of the $\mathbb{Z}_2$ odd particles, can be either the lightest singlet fermion N_1 or the neutral component of the inert scalar doublet η. The detailed phenomenology regarding neutrinos and dark matter for the scotogenic model has been explored in, for instance, refs. [33–37].

A necessary requirement for the viability of the model considered here is that there is no vacuum expectation for the field η ($\langle\eta\rangle = 0$) as otherwise the DM candidate is unstable. The relevant condition for this to hold is that the scalar masses are real (or their squares are positive such that the potential has a stable minimum). In order to ensure that a global minimum exists at finite vacuum expectation value (the potential being bounded from below), the following theoretical conditions have to be satisfied [38],

$$\lambda_1 > 0, \qquad\qquad \lambda_2 > 0\,, \tag{2.15}$$

$$\lambda_3 > -\sqrt{\lambda_1\lambda_2}, \quad \lambda_3 + \lambda_4 - |\lambda_5| > -\sqrt{\lambda_1\lambda_2}\,. \tag{2.16}$$

In addition, all the couplings in the model should be perturbative. Here we take a criterion of perturbativity such that all the couplings are smaller than $\sqrt{4\pi}$. Since the scalar couplings λ_3, λ_4 and λ_5 are correlated with the mass eigenvalues $m_{\eta^+}^2$, m_R^2 and m_I^2, the perturbativity conditions are translated into the following constraints on the masses

$$|\lambda_3| \leq \min\left[\sqrt{4\pi},\ m_{\eta^+}^2/\langle H\rangle^2\right], \quad \left|\frac{m_R^2+m_I^2-2m_{\eta^+}^2}{2\langle H\rangle^2}\right| \leq \sqrt{4\pi}, \quad \left|\frac{m_R^2-m_I^2}{2\langle H\rangle^2}\right| \leq \sqrt{4\pi}\,. \tag{2.17}$$

---

[1]We recall that due to the fact that in this minimal model where only two fermionic singlets (right-handed neutrinos) are considered, the diagonalisation of the neutrino mass matrix leads to a massless active neutrino and thus to only one Majorana CP violating phase, instead of two CP phases in the case of 3 sterile fermions.

3 Electron electric dipole moment

3.1 Experimental status

The current experimental bounds for the charged lepton EDMs are

$$|d_e|/e \leq 8.7 \times 10^{-29}\,\text{cm}, \tag{3.1}$$

$$|d_\mu|/e \leq 1.9 \times 10^{-19}\,\text{cm}, \tag{3.2}$$

$$|d_\tau|/e \leq 4.5 \times 10^{-17}\,\text{cm}. \tag{3.3}$$

These have been measured by ACME Collaboration [26], Muon $g-2$ Collaboration [39] and Belle Collaboration [40], respectively. In particular, the upper bound for the electron EDM is much stronger than the bounds for the muon and tau EDMs. Moreover, the electron EDM is expected to reach $|d_e|/e \sim 10^{-30}\,\text{cm}$ with the next generation experiment of the ACME Collaboration [27]. We focus thus on the electron EDM hereafter, although the analytical formula we derive in this work is general for any charged lepton EDM.

3.2 Computation of electron electric dipole moment

Since EDMs are CP violating observables, relevant couplings for EDMs should be complex to give a non-zero contribution. Note that all the diagrams at one-loop level are proportional to the modulus of the neutrino Yukawa coupling $y_{i\alpha}$. Thus the leading contribution to charged lepton EDMs comes at the two-loop level via the diagrams shown in figure 2. Unlike the case of minimal extensions of the SM via only sterile fermions, where the singlet fermions mix with the left-handed neutrinos as in, for instance, in refs. [25, 29], there are no other two-loop level diagrams than those that are shown in figure 2 contributing to EDMs due to the exact $\mathbb{Z}_2$ symmetry. The derivation of the charged lepton EDMs has been made using FeynCalc for the loop computations [41].

Assuming that the masses of the new particles are much heavier than the charged lepton ones ($m_\alpha \ll m_{\eta^0}, m_{\eta^+}, m_i$), the EDM for a charged lepton ℓ_α can formally be expressed as

$$d_\alpha = -\frac{e\,m_\alpha}{(4\pi)^4 m_{\eta^+}^2} \sum_\beta \sum_{i,j=1}^{2} \left[J_{ij\alpha\beta}^M \sqrt{x_i x_j}\, I_M(x_i, x_j) + J_{ij\alpha\beta}^D I_D(x_i, x_j) \right], \tag{3.4}$$

where $x_i = m_i^2/m_{\eta^+}^2$ ($i = 1, 2$), $I_M(x_i, x_j)$, $I_D(x_i, x_j)$ are the loop functions computed from the two-loop diagrams of figure 2 and the CP phase factors $J_{ij\alpha\beta}^{M,D}$ are defined by

$$J_{ij\alpha\beta}^M \equiv \text{Im}\left(y_{j\alpha}^* y_{j\beta}^* y_{i\beta} y_{i\alpha}\right), \quad J_{ij\alpha\beta}^D \equiv \text{Im}\left(y_{j\alpha}^* y_{j\beta} y_{i\beta}^* y_{i\alpha}\right). \tag{3.5}$$

The first term in eq. (3.4) corresponds to the contribution of diagrams (a1), (a2), (a3), (b1) and (b2), all involving Majorana fermion propagators, they hence pick up the Majorana mass of the singlet fermions in the propagators which can be regarded as lepton number violation; they thus contribute to the Majorana type loop function $I_M(x_i, x_j)$. The second term in eq. (3.4) stems from diagrams (c1) and (c2) with Dirac fermion propagators contributing to the Dirac type loop function $I_D(x_i, x_j)$. The explicit expressions of the
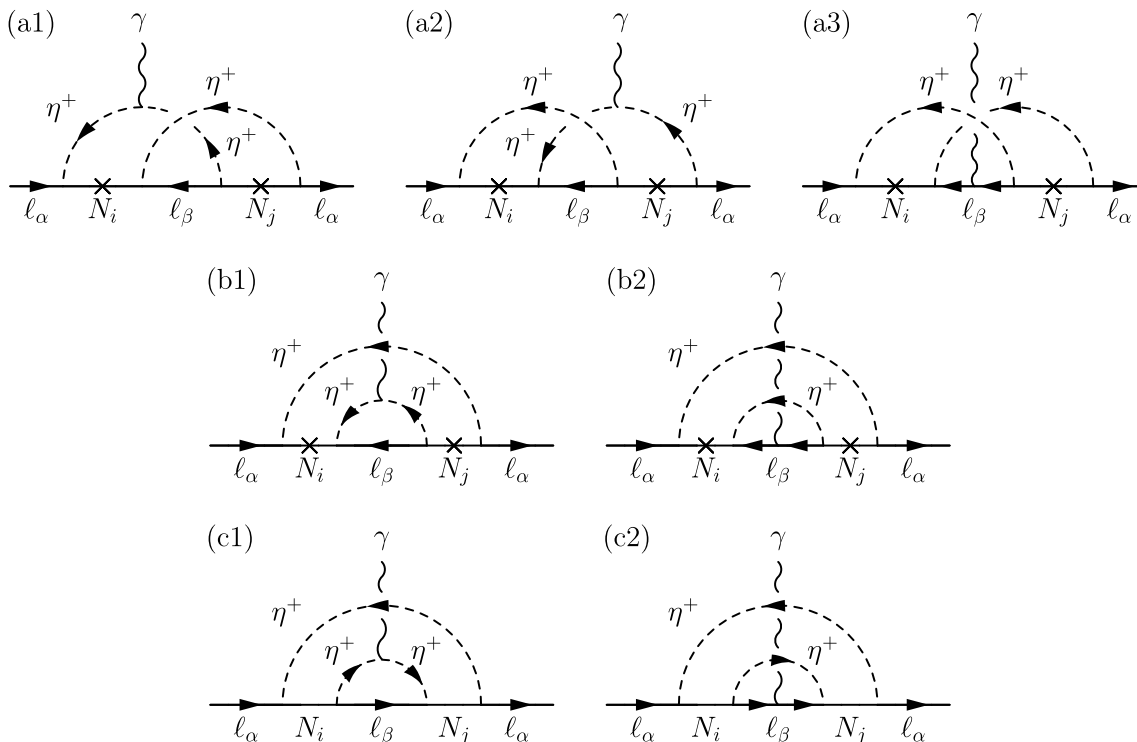
Figure 2. Diagrams for charged lepton EDMs in the minimal scotogenic model.

loop functions $I_{M,D}(x_i, x_j)$ are given in the appendix. Interestingly, one can see from the definition of eq. (3.5) that the phase factors $J_{ij\alpha\beta}^M$ and $J_{ij\alpha\beta}^D$ are anti-symmetric under the exchange of i and j. Thus, only the anti-symmetric part of the loop functions $I_M(x_i, x_j)$ and $I_D(x_i, x_j)$ contributes to the charged lepton EDMs. For this reason, the general formula of eq. (3.4) can be further simplified in our case, where $i, j = 1, 2$, by taking into account the anti-symmetric character of both phase factors and loop functions as follows

$$d_\alpha = -\frac{2\,e\,m_\alpha}{(4\pi)^4 m_{\eta^+}^2} \sum_\beta \left[J_{12\alpha\beta}^M \sqrt{x_1 x_2} I_M(x_1, x_2) + J_{12\alpha\beta}^D I_D(x_1, x_2) \right]. \tag{3.6}$$

As for the expression for the electron EDM ($\alpha = e$), one obtains

$$d_e = -\frac{2\,e\,m_e}{(4\pi)^4 m_{\eta^+}^2} \left[J^M \sqrt{x_1 x_2} I_M(x_1, x_2) + J^D I_D(x_1, x_2) \right], \tag{3.7}$$

with

$$J^M = J_{12e\mu}^M + J_{12e\tau}^M \quad \text{and} \quad J^D = J_{12e\mu}^D + J_{12e\tau}^D. \tag{3.8}$$

The behaviour of the loop functions $I_M(x_i, x_j)$ and $I_D(x_i, x_j)$ that have been numerically evaluated, are shown in figure 3 as a function of x_i for several values of x_j. One can see that both loop functions are of the same order in most of the parameter space, and that the maximal values are $\mathcal{O}(0.01)$ when there is a large hierarchy between the masses of the two sterile states, $x_i \ll x_j$ (i and j can be interchanged, as discussed above). Conversely,
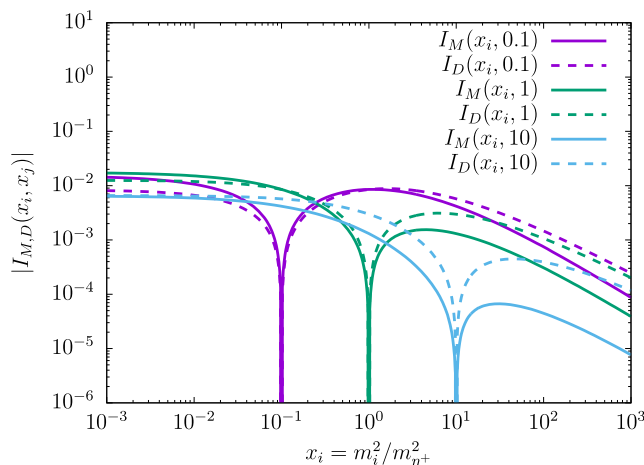
Figure 3. Loop functions $I_M(x_i, x_j)$ and $I_D(x_i, x_j)$ as a function of x_i where $x_j = m_j^2/m_{\eta^+}^2$ is fixed to 0.1, 1 and 10.

these loop functions are suppressed for larger new particle masses, m_i and m_{η^+}. Furthermore, since the loop functions are anti-symmetric under the exchange of $i \leftrightarrow j$, they would also be suppressed if m_i and m_j are extremely degenerate as can be noticed from figure 3.

4 Constraints

Here we summarize the relevant experimental constraints on the minimal scotogenic model we consider.

4.1 Neutrino masses and mixings

We have checked that the considered framework with the parametrization of the neutrino Yukawa couplings given in eq. (2.12) reproduce neutrino data (neutrino mixings and squared neutrino mass differences). We take the following range for the mixing angles and masses, which corresponds to 3σ confidence level [42, 43],

$$0.270 \leq \sin^2\theta_{12} \leq 0.344, \quad 0.382 \leq \sin^2\theta_{23} \leq 0.643, \quad 0.0186 \leq \sin^2\theta_{13} \leq 0.0250, \quad (4.1)$$

$$7.02 \leq \frac{\Delta m_{21}^2}{10^{-5}\,\text{eV}^2} \leq 8.09, \quad 2.317 \leq \frac{\Delta m_{31}^2}{10^{-3}\,\text{eV}^2} \leq 2.607, \quad (4.2)$$

in the case of normal hierarchy, and

$$0.270 \leq \sin^2\theta_{12} \leq 0.344, \quad 0.389 \leq \sin^2\theta_{23} \leq 0.644, \quad 0.0188 \leq \sin^2\theta_{13} \leq 0.0251, \quad (4.3)$$

$$7.02 \leq \frac{\Delta m_{21}^2}{10^{-5}\,\text{eV}^2} \leq 8.09, \quad -2.590 \leq \frac{\Delta m_{32}^2}{10^{-3}\,\text{eV}^2} \leq -2.307, \quad (4.4)$$

in the case of inverted hierarchy.

– 8 –

4.2 Lepton flavour violating processes

The lepton flavour violating (LFV) process $\ell_\alpha \to \ell_\beta\gamma$ imposes a very strong constraint on the model. The branching ratio of the process is computed as [36, 44]

$$\text{Br}\left(\ell_\alpha \to \ell_\beta\gamma\right) = \frac{3\alpha_{\text{em}}}{64\pi^2 G_F^2 m_{\eta^+}^4}\left|\sum_{i=1}^{2} y_{i\alpha}y_{i\beta}^* F_2\left(\frac{m_i^2}{m_{\eta^+}^2}\right)\right|^2 \text{Br}\left(\ell_\alpha \to \ell_\beta\nu_\alpha\overline{\nu_\beta}\right),\qquad (4.5)$$

where G_F is the Fermi constant, α_{em} is the electromagnetic fine structure constant and $F_2(x)$ is the loop function given in ref. [36]. The current experimental upper bounds for these processes [45–47] are,

$$\text{Br}(\mu \to e\gamma) \leq 4.2 \times 10^{-13}\,,\qquad (4.6)$$

$$\text{Br}(\tau \to \mu\gamma) \leq 4.4 \times 10^{-8}\,,\qquad (4.7)$$

$$\text{Br}(\tau \to e\gamma) \leq 3.3 \times 10^{-8}\,,\qquad (4.8)$$

the bound from $\mu \to e\gamma$ being the most constraining one. One can see from eq. (4.5) that if all the Yukawa couplings $y_{i\alpha}$ are assumed to be of the same order of magnitude, the constraint from $\text{Br}(\mu \to e\gamma)$ is translated into

$$|y_{i\alpha}| \lesssim 6 \times 10^{-3}\left(\frac{\text{Max}[m_i, m_{\eta^+}]}{100\,\text{GeV}}\right).\qquad (4.9)$$

Therefore the predicted electron EDM can be roughly estimated by eq. (3.4) taking into account this upper bound on the Yukawa couplings $y_{i\alpha}$. Unfortunately, the predicted electron EDM would be far below the future sensitivity of ACME ($d_e/e \sim 10^{-30}\,\text{cm}$) due to the smallness of the Yukawa couplings. Thus a destructive interference between the contributions of the sterile fermion N_1 and N_2 mediated diagrams for the $\mu \to e\gamma$ process would be necessary to obtain an electron EDM within future sensitivity reach, while being consistent with bounds from LFV processes.

4.3 Electroweak precision data

The inert $SU(2)_L$ scalar doublet η may impact on electroweak precision observables. In particular the oblique STU parameters [48] may receive new contributions due to the existence of the latter scalar doublet. Interestingly, when its CP-even and CP-odd neutral components are nearly degenerate in mass ($m_R \approx m_I$, meaning for small values of the coupling λ_5), the new contributions to the oblique parameters are computed as

$$\Delta S = \frac{1}{12\pi}\log\left(\frac{m_{\eta^0}^2}{m_{\eta^+}^2}\right)\,,\quad \Delta T = \frac{2\sqrt{2}G_F}{(4\pi)^2\alpha_{\text{em}}}F\left(m_{\eta^+}^2, m_{\eta^0}^2\right)\,,\quad \Delta U = \frac{1}{12\pi}G\left(m_{\eta^+}^2, m_{\eta^0}^2\right),$$
$$(4.10)$$

where the loop functions $F(x,y)$ and $G(x,y)$ are given below:

$$F(x,y) = \frac{x+y}{2} - \frac{xy}{x-y}\log\left(\frac{x}{y}\right)\,,\qquad (4.11)$$

$$G(x,y) = -\frac{5x^2 - 22xy + 5y^2}{3(x-y)^2} + \frac{(x+y)(x^2 - 4xy + y^2)}{(x-y)^3}\log\left(\frac{x}{y}\right)\,.\qquad (4.12)$$

The experimental limits on the oblique parameters [49] are given by

$$\Delta S = 0.05 \pm 0.11\,, \quad \Delta T = 0.09 \pm 0.13\,, \quad \Delta U = 0.01 \pm 0.11\,, \tag{4.13}$$

with the correlation coefficients 0.90 between ΔS and ΔT, -0.59 between ΔS and ΔU, and -0.83 between ΔT and ΔU [50]. The constraint of the T-parameter is especially strong, and from eqs. (4.10), (4.11) is translated into the following constraint on the mass splitting [48]

$$\left| m_{\eta^+} - m_{\eta^0} \right| \lesssim 140\,\text{GeV}\,. \tag{4.14}$$

In fact, this constraint is not so important especially when the new scalar particle masses are heavier than a few hundred GeV since the latter mass splitting is proportional to the scalar coupling λ_4 as can be inferred from eqs. (2.3)–(2.6), making the mass splitting bounded from above by perturbativity, see eq. (2.17). This pertubativity requirement provides a stronger bound than eq. (4.14) as discussed in ref. [38]. In addition, if the inert scalar is identified as dark matter, the mass splitting is almost fixed within the bound of eq. (4.14) for a given mass m_{η^0} in order to reproduce the correct relic abundance of dark matter as we will see below.

There are also limits from LEP and LHC where the bounds for slepton searches can be translated into a bound for charged inert scalar η^+. The current ATLAS lower bound translated on m_{η^+} gives $m_{\eta^+} \gtrsim 270\,\text{GeV}$ [51].

4.4 Dark matter searches

Depending on the mass hierarchy between the new particles (neutral fermions and inert scalar particles), this minimal scotogenic model provides two kinds of dark matter candidates, one bosonic candidate corresponding to the neutral component of η and one fermionic candidate corresponding to the lightest Majorana fermion N_1. For both possible cases, we discuss in the following the constraints to reproduce the correct thermal dark matter relic abundance and from dark matter searches through direct and indirect detection for fermionic and inert scalar dark matter separately. In our numerical analysis, the relevant quantities such as cross sections and decay widths are computed with the public code micrOMEGAs [52].

4.4.1 Fermion dark matter

In the case of fermonic dark matter, the lightest neutral fermion N_1 being the potential candidate, the possible annihilation channel determining the dark matter relic abundance is $N_1 N_1 \to \ell_\alpha \overline{\ell_\beta}, \nu_\alpha \nu_\beta$ via the Yukawa coupling $y_{i\alpha}$.[2]

In order to obtain the observed relic abundance, the magnitude of the Yukawa coupling is roughly $y_{i\alpha} \gtrsim 0.1$ taking into account the fact that the dark matter mass should be heavier than the electroweak scale in order to be consistent with the LFV bounds and collider constraints. As discussed in section 4.2, the Yukawa coupling is strongly constrained

---

[2]The co-annihilation channels are also relevant if another fermonic singlet N_2, or if the inert scalar particles η_R, η_I, η^+, are nearly degenerate in mass with N_1, see for instance [53].

by bounds on LFV processes, however these LFV constraints can be evaded with co-annihilation effects for dark matter relic abundance and/or by destructive interference (between the N_1 and N_2 mediated diagrams) in the amplitude of the LFV processes, for example.

Since the fermionic dark matter candidate N_1 interacts only with leptons through the Yukawa coupling $y_{i\alpha}$ and does not interact with quarks and gluons at tree level, there is no substantial constraint from direct detection of dark matter.[3] For indirect detection, a possible signal would be the internal bremsstrahlung processes $N_1 N_1 \to \ell_\alpha \overline{\ell_\beta} \gamma$ because the annihilation cross section for $N_1 N_1 \to \ell_\alpha \overline{\ell_\beta}$ determining the thermal relic abundance is proportional to the small dark matter relative velocity v^2 which is estimated to be of the order of $v \sim 10^{-3}$ in the Galactic center [54–56]. Notice that the current experimental bound for this channel is not very strong and thus does not provide a constraint on the model.

4.4.2 Scalar dark matter

Contrary to the fermionic dark matter case, the inert scalar candidate for dark matter has additional interactions other than the Yukawa coupling $y_{i\alpha}$ such as gauge and scalar interactions, and the relic abundance can be controlled by the corresponding additional couplings. In the following, we identify η_I as the dark matter candidate with a positive scalar coupling λ_5. The inert scalar dark matter in the scotogenic model is basically similar to the inert doublet dark matter [38], the only difference being the existence of the additional Yukawa coupling $y_{i\alpha}$. For the case of the original inert doublet dark matter, there are two allowed regions of dark matter mass: $50\,\text{GeV} \lesssim m_I \lesssim 70\,\text{GeV}$ and $535\,\text{GeV} \lesssim m_I \lesssim 20\,\text{TeV}$ which can reproduce the correct relic abundance and satisfy the relevant constraints [57]. The upper limit of the dark matter mass is derived from the perturbativity requirement, see section 2. For the minimal scotogenic model, the dark matter mass would be similarly restricted in these two regions. Since an extreme fine-tuning between the Yukawa couplings would be required for the light mass region $50\,\text{GeV} \lesssim m_I \lesssim 70\,\text{GeV}$ to be consistent with all the constraints and in order to obtain a large enough electron EDM, we focus in our numerical analysis on the heavy mass region $535\,\text{GeV} \lesssim m_\chi \lesssim 20\,\text{TeV}$.

For direct detection, the elastic scattering with nuclei occurs at tree level via the diagram mediated by the SM Higgs boson if the scalar couplings λ_3, λ_4 and λ_5 are sufficiently large. The gauge interactions also contribute to this process at one-loop level, however the order of magnitude of the latter contribution would be subdominant, $\mathcal{O}(10^{-50})\,\text{cm}^2$ [58]. The current bound for the spin-independent cross section with a proton is given by the XENON1T [59] and the PandaX-II Collaborations [60]. The experimental bound for the spin-independent cross section gives a strong constraint on the scalar couplings, in particular when the dark matter mass is less than a few TeV.

For indirect detection, the continuum gamma-rays are generated from the annihilation modes $\eta_I \eta_I \to WW, ZZ, hh$ and subsequent decays of the final state particles, providing a constraint on the model. In particular, if the dark matter mass is much heavier than

---

[3]Notice that if N_1 and N_2 are nearly degenerate and if the Yukawa coupling is complex as in our case, inelastic scattering process with nucleons can be induced at loop level [35].

the masses of the SM gauge and Higgs bosons, the annihilation cross sections for these channels are enhanced by non-perturbative Sommerfeld effect, and in this case, the constraint becomes stronger. We include in our analysis the Sommerfeld effect, and impose the experimental bound obtained from the H.E.S.S. Collaboration [61].[4] The detailed discussion for the Sommerfeld effect and the experimental bounds can be found in ref. [57] and references therein.

5 Numerical analysis

In this section, we investigate viable parameter space in the case of fermionic dark matter and scalar dark matter below, considering in each case both normal and inverted ordering of the light neutrino spectrum. The results are displayed and discussed separately for the cases of fermionic and scalar dark matter since the corresponding phenomenological constraints for dark matter are different.

5.1 Fermionic dark matter

As motivated above, we consider in this case where the lightest fermonic singlet is the dark matter candidate, the following intervals in our numerical computations:

$$100\,\text{GeV} \leq m_1 \leq 100\,\text{TeV}, \qquad 1 \leq \frac{m_2}{m_1}, \frac{m_{\eta^0}}{m_1}, \frac{m_{\eta^+}}{m_1} \leq 10, \tag{5.1}$$

$$0 \leq \delta_{\text{CP}}, \varphi_{\text{CP}}, \eta_{\text{CP}} < 2\pi, \qquad 0 \leq |\sin\xi| \leq 1, \qquad |\lambda_3|, |\lambda_4| \leq \sqrt{4\pi}. \tag{5.2}$$

The intervals for the different masses in eq. (5.1) cover most of the parameter space. Notice that the ratio between the mass of the singlet fermion N_1 and the inert scalar doublet cannot be very large, this is due to the fact that the annihilation cross section for $N_1 N_1 \to \ell_\alpha \overline{\ell_\beta}, \nu_\alpha \nu_\beta$, determining the relic abundance, is mediated by the inert scalar doublet, and is suppressed if the scalars are too heavy.

The numerical results are shown in figures 4 and 5 for normal and inverted hierarchy of the light neutrino mass spectrum, respectively, where the electron EDM, the scalar couplings λ_5, λ_3 and λ_4 the mass ratios between the new particles (m_2/m_1, m_{η^0}/m_1 and m_{η^+}/m_1), the phase factors $|J^M|$, $|J^D|$ and the CP phase η_{CP} (= Arg(ξ)) are displayed as a function of the dark matter mass m_1.

From the left-top panels in figures 4 and 5, one can see that the electron EDM can be larger than the future prospect of the next generation experiment of the ACME collaboration [27] (dashed horizontal black line) when the dark matter mass is lighter than 4 TeV. The predicted electron EDM can be even slightly larger in the case of inverted hierarchy as can be seen in the first left panel of figure 5.

The scalar couplings $|\lambda_3|$ and $|\lambda_4|$, and λ_5 as a function of the dark matter mass m_1 are displayed on the right-top and left-middle panels of figures 4 and 5. The orange coloured points for $|\lambda_3|$ and λ_5, and the red coloured points for $|\lambda_4|$ denote electron EDM larger than the future prospect $|d_e|/e \geq 10^{-30}$ cm. One can find that the typical magnitude of the coupling λ_5 is $10^{-11} \lesssim \lambda_5 \lesssim 10^{-8}$ to satisfy all the constraints. In order to have the

---

[4]The bound for the annihilation cross section may be updated with the latest H.E.S.S. measurement [62].
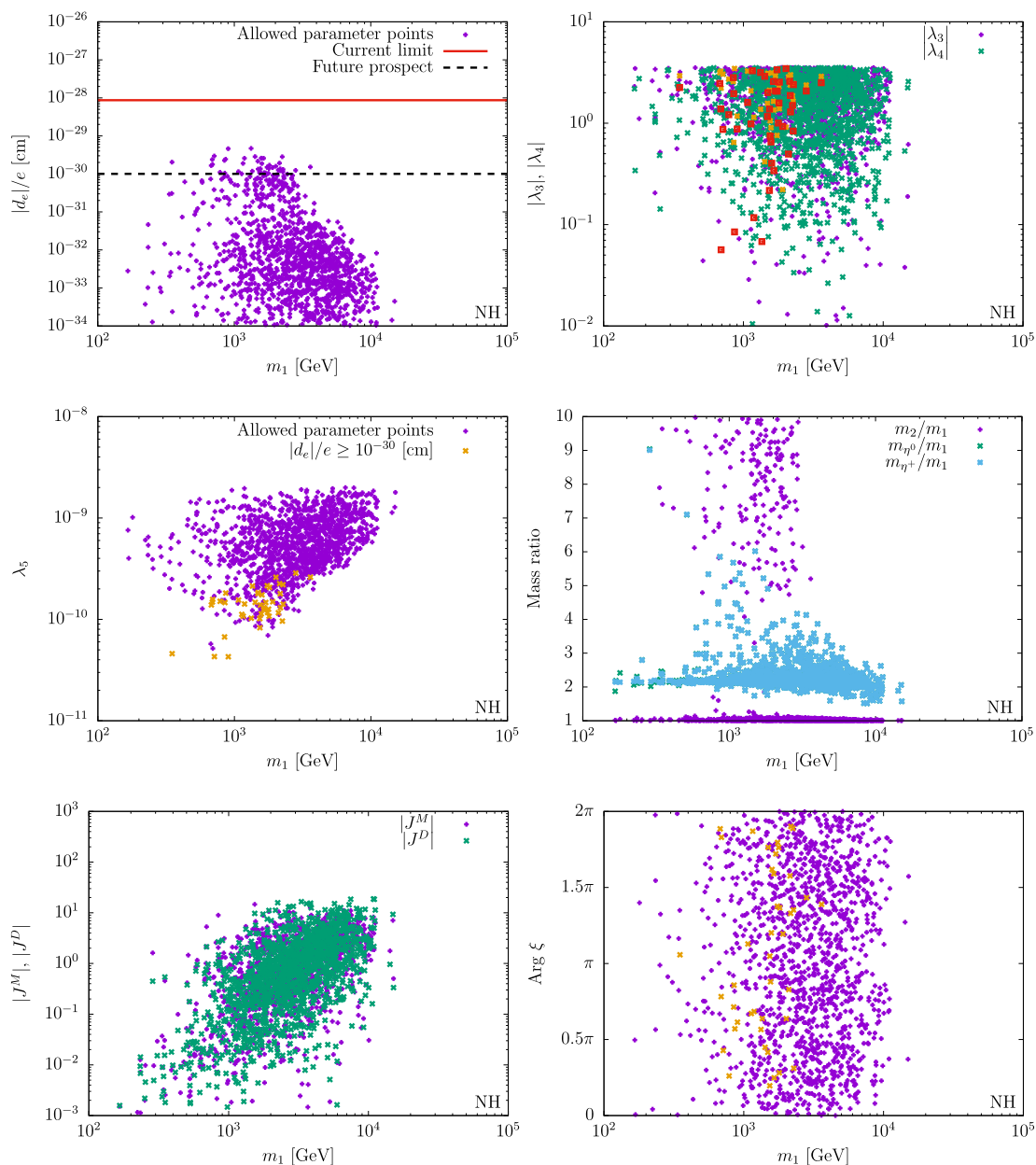
Figure 4. Numerical results for fermionic dark matter in the case of normal hierarchy for the light neutrino spectrum. Each point complies with all the constraints discussed in section 4.

electron EDM within future sensitivity reach of ACME, the coupling λ_5 should be in the range $\lambda_5 \lesssim 3 \times 10^{-10}$ in the case of normal ordering for the light neutrino spectrum. In the case of the inverted ordering, the coupling λ_5 can be a few factor larger than that in the case of normal hierarchy, and is bounded from below by the perturbativity condition on the Yukawa coupling since the coupling λ_5 behaves like $\lambda_5 \propto y^{-2}$ as one can see from eq. (2.10) and (2.12). On the other hand, it is bounded from above because of the condition from the dark matter relic abundance. This can be understood since $\Omega_{\text{DM}} h^2 \propto |y|^{-4} \propto \lambda_5^2$.
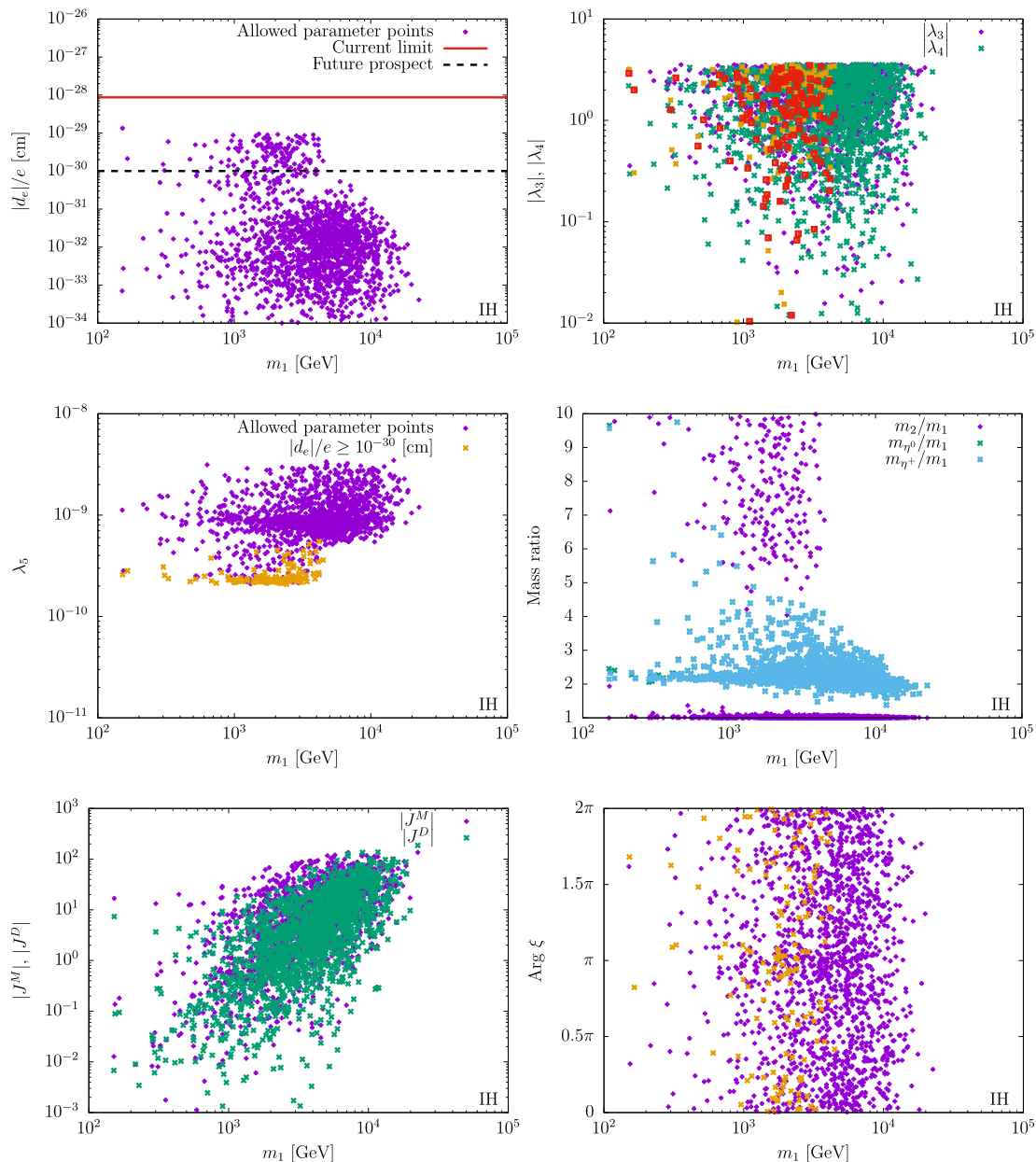
Figure 5. Numerical results for fermion dark matter in the case of inverted hierarchy for the light neutrino spectrum. Each point complies with all the constraints discussed in section 4.

From the right-middle plots of figures 4 and 5, one can see that the charged inert scalar mass is close to $2 \lesssim m_{\eta^+}/m_1 \lesssim 4$ for most of the parameter points. This is because the branching ratios of the LFV processes given by eq. (4.5) are drastically reduced when the mass of the charged inert scalar m_{η^+} is in this range due to destructive interference between the N_1 and N_2 mediated diagrams. Because of this, the strong constraint of the LFV processes can be evaded.

On the left-bottom panels of figures 4 and 5, we display the phase factors $|J^M|$ and $|J^D|$ as a function of the dark matter mass. One can find that the phase factors $|J^M|$ and $|J^D|$ are always of the same order in both cases of normal and inverted hierarchies of the light neutrino mass spectrum. Although the explicit form of the phase factors J^M and J^D is not shown here due to complexity (the definition being given in eq. (3.5) and (3.8)), we found that the phase factor behaves as $J^M, J^D \propto \sin\theta_{13}$ in the case of normal hierarchy of the light neutrino spectrum. On the other hand, J^M and J^D can be maximal $J^M, J^D \sim (\sqrt{4\pi})^4 \sim 100$ in the inverted hierarchy case because there is no $\sin\theta_{13}$ factor of supression. Notice that we have numerically checked that if one assumes $\eta_{\rm CP} = 0$, the phase factor $|J^D|$ is suppressed with about two orders of magnitude compared to $|J^M|$, in the inverted hierarchy case.

The right-bottom panels in figure 4 and 5 show $\mathrm{Arg}(\xi) = \eta_{\rm CP}$ as a function of m_1 where the orange points denote the allowed parameter points with $|d_e|/e \geq 10^{-30}$ cm. One can see a small dependence on $\eta_{\rm CP}$ of the maximum dark matter mass m_1 allowed by all the constraints in the plots while the predicted electron EDM is below the future sensitivity for a large dark matter mass.

5.2 The case of inert scalar dark matter

In the case in which the neutral component of the inert scalar doublet η is the dark matter candidate, one expects a larger viable parameter space than in the case of fermonic dark matter (see section above). This is due to the fact that the inert scalar dark matter can annihilate into $\eta^{0\dagger}\eta^0 \to WW$, ZZ, $f\overline{f}$, hh, other than $\eta^{0\dagger}\eta^0 \to \ell_\alpha\overline{\ell_\beta}, \nu_\alpha\nu_\beta$ via the Yukawa coupling $y_{i\alpha}$, which are relevant to reproduce the observed relic abundance of dark matter.

We thus explore a larger range for the new particles mass ratios and consider the following intervals in our numerical computations:

$$100\,\mathrm{GeV} \leq m_{\eta^0} \leq 100\,\mathrm{TeV}, \qquad 1 \leq \frac{m_1}{m_{\eta^0}}, \frac{m_2}{m_{\eta^0}}, \frac{m_{\eta^+}}{m_{\eta^0}} \leq 1000, \tag{5.3}$$

$$0 \leq \delta_{\rm CP}, \varphi_{\rm CP}, \eta_{\rm CP} < 2\pi, \quad 0 \leq |\sin\xi| \leq 1, \quad |\lambda_3|, |\lambda_4| \leq \sqrt{4\pi}. \tag{5.4}$$

The numerical results for the bosonic dark matter case are shown in figures 6 and 7 for normal and inverted hierarchy of the light neutrino mass spectrum, respectively, where the electron EDM, the scalar couplings $|\lambda_3|, |\lambda_4|$ and λ_5, the mass ratios between the new particles (m_i/m_{η^0} and m_{η^+}/m_{η^0}), the phase factors $|J^M|, |J^D|$, and $\mathrm{Arg}(\xi) = \eta_{\rm CP}$ are plotted as a function of the dark matter mass m_{η^0}.

From the left-top panels in figures 6 and 7 one can see that unlike the case of fermonic dark matter, the predicted electron EDM cannot reach the future sensitivity $|d_e|/e = 10^{-30}$ cm of the next generation of ACME collaboration. One can see that the phase factors $|J^M|$ and $|J^D|$ displayed on the left-bottom panels of figures 6 and 7 as a function of the dark matter mass, are almost of the same order as the corresponding ones in the case of fermion dark matter, and the dark matter mass region is also similar. Therefore the difference between the predicted electron EDM between these cases (bosonic and fermonic dark matter) can only be due to the behaviour of the loop functions I_M and I_D (presented in figure 3).
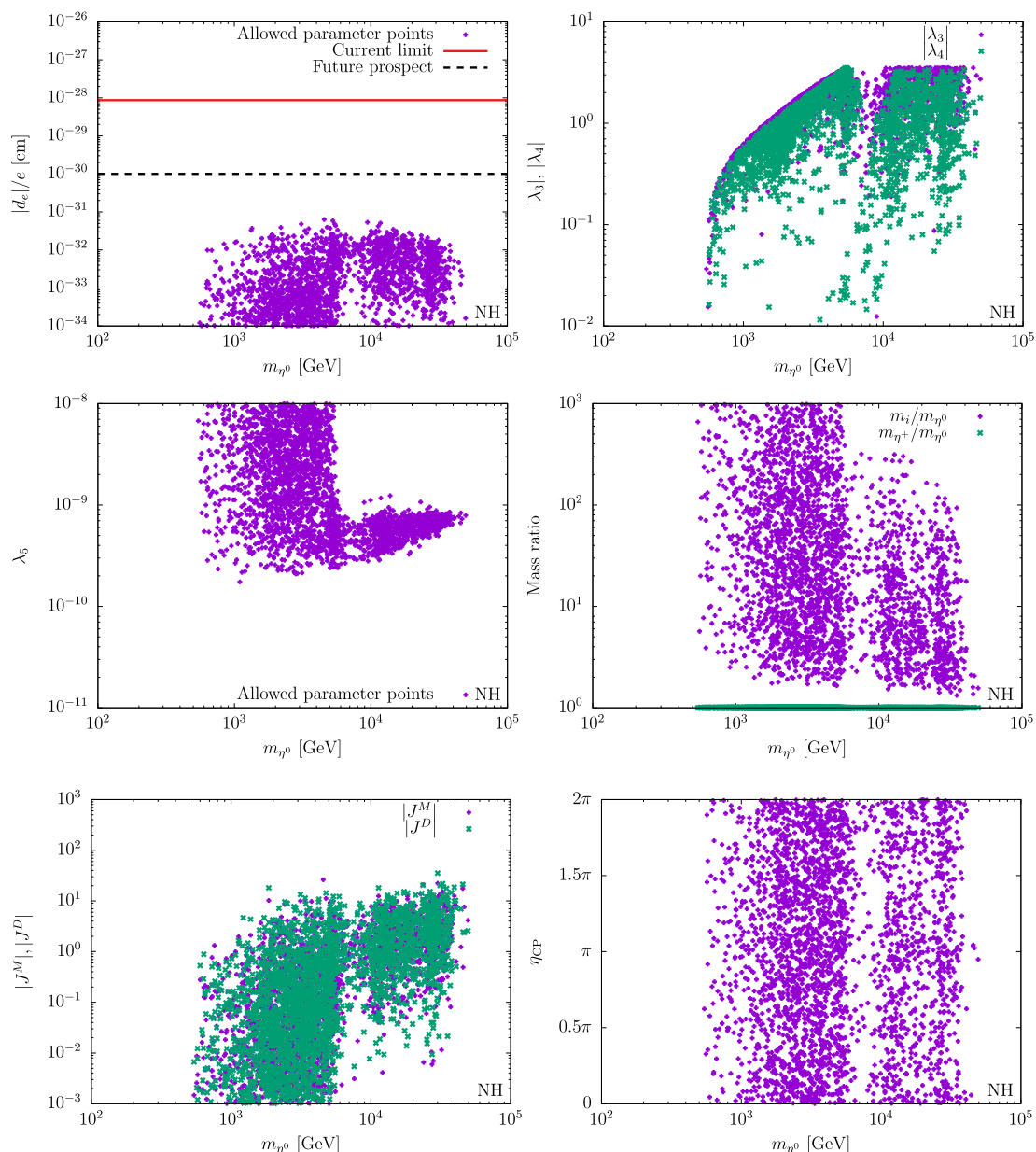
Figure 6. Numerical results for scalar dark matter in the case of normal ordering of the light neutrino mass spectrum. Each point complies with all the constraints discussed in section 4.

The scalar couplings $|\lambda_3|$, $|\lambda_4|$ and λ_5 are displayed on the right-top and left-middle panels of figures 6 and 7. For dark matter mass lighter than $m_{\eta^0} \lesssim 1\,\mathrm{TeV}$, the annihilation cross sections for the channels into the gauge bosons are large enough in order to obtain the observed relic abundance, and the scalar couplings $|\lambda_3|$ and $|\lambda_4|$ have to be subdominant. For $m_{\eta^0} \gtrsim 1\,\mathrm{TeV}$, the scalar couplings $|\lambda_3|$ and $|\lambda_4|$ starts to be $\mathcal{O}(1)$, and reach the perturbativity bound $\sqrt{4\pi}$ at around $m_{\eta^0} \sim 5\,\mathrm{TeV}$. The scalar coupling λ_5 ($\propto y^{-2}$) can be larger compared to the case of fermionic dark matter since the inert scalar dark matter
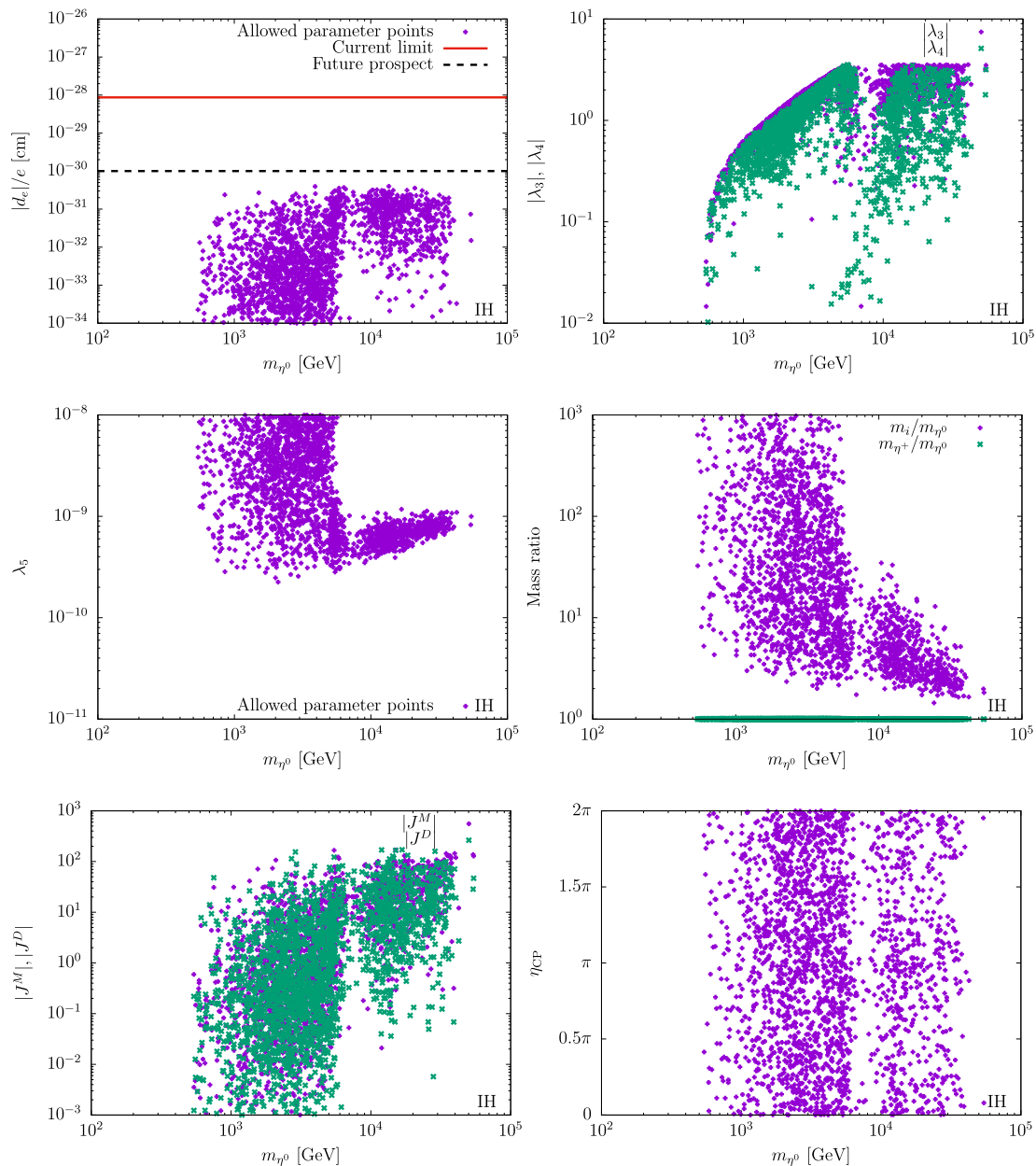
Figure 7. Numerical results for scalar dark matter in the case of inverted hierarchy for the light neutrino mass spectrum. Each point complies with all the constraints discussed in section 4.

has the additional gauge and scalar interactions to reproduce the correct relic abundance. As can be seen, the parameter space of λ_5 drastically changes around $m_{\eta^0} \sim 6\,\text{TeV}$. This implies that the correct relic abundance cannot be obtained without the Yukawa coupling $y_{i\alpha}$ for $m_{\eta^0} \gtrsim 6\,\text{TeV}$. While only the region of $10^{-11} \le \lambda_5 \le 10^{-8}$ is shown in the plots, we have checked that the scalar coupling λ_5 can be larger. However in this case, the predicted electron EDM is still too small due to the smallness of the Yukawa coupling.

From the right-middle plots of figures 6 and 7, one can find that the fermion masses can be much larger than the dark matter mass while the charged inert scalar should be almost degenerate with the dark matter mass (green points). The region of $m_i/m_{\eta^0} \lesssim 2$ is excluded by the several LFV constraints.

The right-bottom plots show $\eta_{\rm CP}$ dependence of dark matter mass allowed by all the constraints, and these plots are similar to the ones obtained in the case of fermionic dark matter. In all the plots in figure 6 and 7, the dark matter mass region $6\,{\rm TeV} \lesssim m_{\eta^0} \lesssim 9\,{\rm TeV}$ is strongly constrained by gamma-ray observations for dark matter indirect detection due to the peak of the Sommerfeld enhancement for the annihilation cross sections.

6 Conclusions and discussions

We have computed the charged lepton EDMs in the (minimal) scotogenic model whose leading contribution is induced at two-loop level. The numerical computation has been conducted taking into account all the various relevant experimental and theoretical constraints on the parameter space of the model. We have found that the predicted electron EDM could reach the future sensitivity $|d_e|/e = 10^{-30}\,{\rm cm}$ of the next generation of the ACME, consistently complying with all the constraints, only when the lightest singlet fermion is identified as a dark matter candidate. Notice that the predicted electron EDM is actually larger than what was obtained in several seesaw models, as the case of the inverse seesaw where neutrino masses are generated at tree level [29]. In the case of normal hierarchy of the light neutrino mass spectrum, the CP phase factors $|J^M|$ and $|J^D|$ complying with all the constraints are one order of magnitude smaller than the case of inverted hierarchy. However the magnitude of the predicted electron EDM is eventually almost of the same order for both cases.

The electron EDM which has been calculated in this paper may be correlated with another observables related to CP violation such as the BAU. In the scotogenic model, the generation of BAU via resonant leptogenesis has been discussed in [63, 64]. Correlating the BAU, the radiative neutrino mass generation and a fermonic dark matter scenario, while having an electron EDM within ACME reach is certainly very interesting and we leave this possibility for a future project.

A Loop functions

Here we give the loop functions which appear in the formula of charged lepton EDMs at two-loop level in eq. (3.4). The contribution from the pair of the diagrams (a1) and (a2), and the contribution from the diagram (a3) are given by

$$
I_{1+2}^M(x_i, x_j) = \int_0^1 \prod_{a=1}^4 ds_a \, \delta\left(\sum_{a=1}^4 s_a - 1\right) \int_0^1 \prod_b^4 dt_b \, \delta\left(\sum_{b=1}^4 t_b - 1\right)
$$
$$
\times \frac{s_1 s_4 (1 - t_3 - t_4)^2 - t_1 t_2 (1 - s_2 - s_3)^2}{2\left[(s_2 + s_3)(1 - s_2 - s_3)(t_1 x_i + t_2) + (t_3 + t_4)(s_1 x_j + s_4)\right]^2}, \quad (A.1)
$$
$$
I_3^M(x_i, x_j) = \int_0^1 \prod_{a=1}^3 ds_a \, \delta\left(\sum_{a=1}^3 s_a - 1\right) \int_0^1 \prod_b^4 dt_b \, \delta\left(\sum_{b=1}^4 t_b - 1\right)
$$
$$
\times \frac{s_1 s_2 (1 - t_4)(-t_1 + s_2 t_1 - s_3 t_4)}{\left[s_2(1 - s_2)(t_1 x_i + t_2 + t_3) + t_4(s_1 x_j + s_3)\right]^2}. \quad (A.2)
$$

For the diagrams (b1) and (b2), each diagram gives non-zero contribution, however one can find that these can exactly be the same expressions with opposite sign in the limit $x_\alpha, x_\beta \to 0$. Thus the contributions from (b1) and (b2) cancel with each other, and the whole Majorana type loop function is given by $I_M(x_i, x_j) = I_{1+2}^M(x_i, x_j) + I_3^M(x_i, x_j)$.

The diagrams (c1) and (c2) providing the Dirac type contribution include a divergence for each diagram. However the divergence cancels out and the whole loop function is finite as given by

$$
I^D(x_i, x_j) = \int_0^1 \prod_{a=1}^3 ds_a \, \delta\left(\sum_{a=1}^3 s_a - 1\right) \int_0^1 \prod_b^3 dt_b \, \delta\left(\sum_{b=1}^3 t_b - 1\right) \frac{t_1(t_2 - t_3)}{2\left[t_1 + t_2 x_i + t_3 x_j\right]}
$$
$$
+ \int_0^1 \prod_{a=1}^3 ds_a \, \delta\left(\sum_{a=1}^3 s_a - 1\right) \int_0^1 \prod_b^4 dt_b \, \delta\left(\sum_{b=1}^4 t_b - 1\right)
$$
$$
\times \frac{s_1(1 + 4s_1)}{2} \frac{t_1(t_2 - t_3)}{\left[s_1(t_1 + t_2 x_i + t_3 x_j) + t_4\right]^2}. \quad (A.3)
$$

References

[1] P. Minkowski, $\mu \to e\gamma$ *at a Rate of One Out of* 10^9 *Muon Decays?*, [*Phys. Lett.* **B 67** (1977) 421](#) [INSPIRE].

[2] T. Yanagida, *Horizontal symmetry and masses of neutrinos*, *Conf. Proc.* **C 7902131** (1979) 95 [INSPIRE].

[3] M. Gell-Mann, P. Ramond and R. Slansky, *Complex Spinors and Unified Theories*, *Conf. Proc.* **C 790927** (1979) 315 [[arXiv:1306.4669](#)] [INSPIRE].

[4] S.L. Glashow, *The Future of Elementary Particle Physics*, *NATO Sci. Ser.* **B 61** (1980) 687 [INSPIRE].

[5] R.N. Mohapatra and G. Senjanović, *Neutrino Mass and Spontaneous Parity Violation*, *Phys. Rev. Lett.* **44** (1980) 912 [INSPIRE].

[6] J. Schechter and J.W.F. Valle, *Neutrino Masses in* SU(2) × U(1) *Theories*, *Phys. Rev.* **D 22** (1980) 2227 [INSPIRE].

[7] J. Schechter and J.W.F. Valle, *Neutrino Decay and Spontaneous Violation of Lepton Number*, *Phys. Rev.* **D 25** (1982) 774 [INSPIRE].

[8] R. Foot, H. Lew, X.G. He and G.C. Joshi, *Seesaw Neutrino Masses Induced by a Triplet of Leptons*, *Z. Phys.* **C 44** (1989) 441 [INSPIRE].

[9] R.N. Mohapatra and J.W.F. Valle, *Neutrino Mass and Baryon Number Nonconservation in Superstring Models*, *Phys. Rev.* **D 34** (1986) 1642 [INSPIRE].

[10] S.M. Barr, *A Different seesaw formula for neutrino masses*, *Phys. Rev. Lett.* **92** (2004) 101601 [hep-ph/0309152] [INSPIRE].

[11] M. Malinsky, J.C. Romao and J.W.F. Valle, *Novel supersymmetric* SO(10) *seesaw mechanism*, *Phys. Rev. Lett.* **95** (2005) 161801 [hep-ph/0506296] [INSPIRE].

[12] PLANCK collaboration, P.A.R. Ade et al., *Planck 2013 results. XVI. Cosmological parameters*, *Astron. Astrophys.* **571** (2014) A16 [arXiv:1303.5076] [INSPIRE].

[13] M. Fukugita and T. Yanagida, *Baryogenesis Without Grand Unification*, *Phys. Lett.* **B 174** (1986) 45 [INSPIRE].

[14] A. Ali, A.V. Borisov and N.B. Zamorin, *Majorana neutrinos and same sign dilepton production at LHC and in rare meson decays*, *Eur. Phys. J.* **C 21** (2001) 123 [hep-ph/0104123] [INSPIRE].

[15] A. Atre, V. Barger and T. Han, *Upper bounds on lepton-number violating processes*, *Phys. Rev.* **D 71** (2005) 113014 [hep-ph/0502163] [INSPIRE].

[16] A. Atre, T. Han, S. Pascoli and B. Zhang, *The Search for Heavy Majorana Neutrinos*, *JHEP* **05** (2009) 030 [arXiv:0901.3589] [INSPIRE].

[17] M. Chrzaszcz, *Searches for LFV and LNV Decays at LHCb*, in *7th International Workshop on the CKM Unitarity Triangle (CKM 2012)*, Cincinnati, Ohio, U.S.A., September 28–October 2, 2012 [arXiv:1301.2088] [INSPIRE].

[18] F.F. Deppisch, P.S. Bhupal Dev and A. Pilaftsis, *Neutrinos and Collider Physics*, *New J. Phys.* **17** (2015) 075019 [arXiv:1502.06541] [INSPIRE].

[19] Y. Cai, T. Han, T. Li and R. Ruiz, *Lepton-Number Violation: Seesaw Models and Their Collider Tests*, arXiv:1711.02180 [INSPIRE].

[20] A. Abada, V. De Romeri, M. Lucente, A.M. Teixeira and T. Toma, *Effective Majorana mass matrix from tau and pseudoscalar meson lepton number violating decays*, *JHEP* **02** (2018) 169 [arXiv:1712.03984] [INSPIRE].

[21] A. de Gouvêa and S. Gopalakrishna, *Low-energy neutrino Majorana phases and charged-lepton electric dipole moments*, *Phys. Rev.* **D 72** (2005) 093008 [hep-ph/0508148] [INSPIRE].

[22] D. Ng and J.N. Ng, *A Note on Majorana neutrinos, leptonic CKM and electron electric dipole moment*, *Mod. Phys. Lett.* **A 11** (1996) 211 [hep-ph/9510306] [INSPIRE].

[23] J.P. Archambault, A. Czarnecki and M. Pospelov, *Electric dipole moments of leptons in the presence of Majorana neutrinos*, *Phys. Rev.* **D 70** (2004) 073006 [`hep-ph/0406089`] [InSPIRE].

[24] W.-F. Chang and J.N. Ng, *Charged lepton electric dipole moments from TeV scale right-handed neutrinos*, *New J. Phys.* **7** (2005) 65 [`hep-ph/0411201`] [InSPIRE].

[25] A. Abada and T. Toma, *Electric Dipole Moments of Charged Leptons with Sterile Fermions*, *JHEP* **02** (2016) 174 [`arXiv:1511.03265`] [InSPIRE].

[26] ACME collaboration, J. Baron et al., *Order of Magnitude Smaller Limit on the Electric Dipole Moment of the Electron*, *Science* **343** (2014) 269 [`arXiv:1310.7534`] [InSPIRE].

[27] W.C. Griffith, *Measurements and implications of EDMs*, plenary talk at *Interplay between Particle & Astroparticle physics 2014*, Queen Mary University of London, 18–22 August 2014 [https://indico.ph.qmul.ac.uk/indico/conferenceDisplay.py?confId=1].

[28] A. Abada and M. Lucente, *Looking for the minimal inverse seesaw realisation*, *Nucl. Phys.* **B 885** (2014) 651 [`arXiv:1401.1507`] [InSPIRE].

[29] A. Abada and T. Toma, *Electron electric dipole moment in Inverse Seesaw models*, *JHEP* **08** (2016) 079 [`arXiv:1605.07643`] [InSPIRE].

[30] E. Ma, *Verifiable radiative seesaw mechanism of neutrino mass and dark matter*, *Phys. Rev.* **D 73** (2006) 077301 [`hep-ph/0601225`] [InSPIRE].

[31] G. 't Hooft, *Naturalness, chiral symmetry, and spontaneous chiral symmetry breaking*, *NATO Sci. Ser.* **B 59** (1980) 135 [InSPIRE].

[32] J.A. Casas and A. Ibarra, *Oscillating neutrinos and* $\mu \to e, \gamma$, *Nucl. Phys.* **B 618** (2001) 171 [`hep-ph/0103065`] [InSPIRE].

[33] J. Kubo, E. Ma and D. Suematsu, *Cold Dark Matter, Radiative Neutrino Mass,* $\mu \to e\gamma$ *and Neutrinoless Double Beta Decay*, *Phys. Lett.* **B 642** (2006) 18 [`hep-ph/0604114`] [InSPIRE].

[34] D. Suematsu, T. Toma and T. Yoshida, *Reconciliation of CDM abundance and* $\mu \to e\gamma$ *in a radiative seesaw model*, *Phys. Rev.* **D 79** (2009) 093004 [`arXiv:0903.0287`] [InSPIRE].

[35] D. Schmidt, T. Schwetz and T. Toma, *Direct Detection of Leptophilic Dark Matter in a Model with Radiative Neutrino Masses*, *Phys. Rev.* **D 85** (2012) 073009 [`arXiv:1201.0906`] [InSPIRE].

[36] T. Toma and A. Vicente, *Lepton Flavor Violation in the Scotogenic Model*, *JHEP* **01** (2014) 160 [`arXiv:1312.2840`] [InSPIRE].

[37] H. Davoudiasl and I.M. Lewis, *Right-Handed Neutrinos as the Origin of the Electroweak Scale*, *Phys. Rev.* **D 90** (2014) 033003 [`arXiv:1404.6260`] [InSPIRE].

[38] T. Hambye, F.S. Ling, L. Lopez Honorez and J. Rocher, *Scalar Multiplet Dark Matter*, *JHEP* **07** (2009) 090 [*Erratum ibid.* **05** (2010) 066] [`arXiv:0903.4010`] [InSPIRE].

[39] Muon (g-2) collaboration, G.W. Bennett et al., *An Improved Limit on the Muon Electric Dipole Moment*, *Phys. Rev.* **D 80** (2009) 052008 [`arXiv:0811.1207`] [InSPIRE].

[40] Belle collaboration, K. Inami et al., *Search for the electric dipole moment of the tau lepton*, *Phys. Lett.* **B 551** (2003) 16 [`hep-ex/0210066`] [InSPIRE].

[41] R. Mertig, M. Böhm and A. Denner, *FEYN CALC: Computer algebraic calculation of Feynman amplitudes*, *Comput. Phys. Commun.* **64** (1991) 345 [InSPIRE].

[42] M.C. Gonzalez-Garcia, M. Maltoni and T. Schwetz, *Updated fit to three neutrino mixing: status of leptonic CP-violation*, *JHEP* **11** (2014) 052 [arXiv:1409.5439] [INSPIRE].

[43] I. Esteban, M.C. Gonzalez-Garcia, M. Maltoni, I. Martinez-Soler and T. Schwetz, *Updated fit to three neutrino mixing: exploring the accelerator-reactor complementarity*, *JHEP* **01** (2017) 087 [arXiv:1611.01514] [INSPIRE].

[44] M. Lindner, M. Platscher and F.S. Queiroz, *A Call for New Physics: The Muon Anomalous Magnetic Moment and Lepton Flavor Violation*, *Phys. Rept.* **731** (2018) 1 [arXiv:1610.06587] [INSPIRE].

[45] MEG collaboration, J. Adam et al., *New constraint on the existence of the $\mu^+ \to e^+\gamma$ decay*, *Phys. Rev. Lett.* **110** (2013) 201801 [arXiv:1303.0754] [INSPIRE].

[46] PARTICLE DATA GROUP collaboration, C. Patrignani et al., *Review of Particle Physics*, *Chin. Phys.* **C 40** (2016) 100001 [INSPIRE].

[47] MEG collaboration, A.M. Baldini et al., *Search for the lepton flavour violating decay $\mu^+ \to e^+\gamma$ with the full dataset of the MEG experiment*, *Eur. Phys. J.* **C 76** (2016) 434 [arXiv:1605.05081] [INSPIRE].

[48] R. Barbieri, L.J. Hall and V.S. Rychkov, *Improved naturalness with a heavy Higgs: An Alternative road to LHC physics*, *Phys. Rev.* **D 74** (2006) 015007 [hep-ph/0603188] [INSPIRE].

[49] PARTICLE DATA GROUP collaboration, C. Patrignani et al., *Review of Particle Physics*, *Chin. Phys.* **C 40** (2016) 100001 [INSPIRE].

[50] GFITTER GROUP collaboration, M. Baak et al., *The global electroweak fit at NNLO and prospects for the LHC and ILC*, *Eur. Phys. J.* **C 74** (2014) 3046 [arXiv:1407.3792] [INSPIRE].

[51] ATLAS collaboration, *Search for direct production of charginos, neutralinos and sleptons in final states with two leptons and missing transverse momentum in pp collisions at $\sqrt{s} = 8\,TeV$ with the ATLAS detector*, *JHEP* **05** (2014) 071 [arXiv:1403.5294] [INSPIRE].

[52] G. Bélanger, F. Boudjema, A. Pukhov and A. Semenov, *MicrOMEGAs4.1: two dark matter candidates*, *Comput. Phys. Commun.* **192** (2015) 322 [arXiv:1407.6129] [INSPIRE].

[53] M. Klasen, C.E. Yaguna, J.D. Ruiz-Alvarez, D. Restrepo and O. Zapata, *Scalar dark matter and fermion coannihilations in the radiative seesaw model*, *JCAP* **04** (2013) 044 [arXiv:1302.5298] [INSPIRE].

[54] T. Bringmann, L. Bergstrom and J. Edsjo, *New Gamma-Ray Contributions to Supersymmetric Dark Matter Annihilation*, *JHEP* **01** (2008) 049 [arXiv:0710.3169] [INSPIRE].

[55] H. Okada and T. Toma, *Effect of Degenerate Particles on Internal Bremsstrahlung of Majorana Dark Matter*, *Phys. Lett.* **B 750** (2015) 266 [arXiv:1411.4858] [INSPIRE].

[56] M. Garny, A. Ibarra and S. Vogl, *Signatures of Majorana dark matter with t-channel mediators*, *Int. J. Mod. Phys.* **D 24** (2015) 1530019 [arXiv:1503.01500] [INSPIRE].

[57] C. Garcia-Cely, M. Gustafsson and A. Ibarra, *Probing the Inert Doublet Dark Matter Model with Cherenkov Telescopes*, *JCAP* **02** (2016) 043 [arXiv:1512.02801] [INSPIRE].

[58] M. Farina, D. Pappadopulo and A. Strumia, *A modified naturalness principle and its experimental tests*, *JHEP* **08** (2013) 022 [arXiv:1303.7244] [INSPIRE].

[59] XENON collaboration, E. Aprile et al., *First Dark Matter Search Results from the XENON1T Experiment*, *Phys. Rev. Lett.* **119** (2017) 181301 [`arXiv:1705.06655`] [ɪɴSPIRE].

[60] PandaX-II collaboration, X. Cui et al., *Dark Matter Results From 54-Ton-Day Exposure of PandaX-II Experiment*, *Phys. Rev. Lett.* **119** (2017) 181302 [`arXiv:1708.06917`] [ɪɴSPIRE].

[61] H.E.S.S. collaboration, A. Abramowski et al., *Search for a Dark Matter annihilation signal from the Galactic Center halo with H.E.S.S*, *Phys. Rev. Lett.* **106** (2011) 161301 [`arXiv:1103.3266`] [ɪɴSPIRE].

[62] H.E.S.S. collaboration, H. Abdalla et al., *H.E.S.S. Limits on Linelike Dark Matter Signatures in the* 100 *GeV to* 2 *TeV Energy Range Close to the Galactic Center*, *Phys. Rev. Lett.* **117** (2016) 151302 [`arXiv:1609.08091`] [ɪɴSPIRE].

[63] S. Kashiwase and D. Suematsu, *Baryon number asymmetry and dark matter in the neutrino mass model with an inert doublet*, *Phys. Rev.* **D 86** (2012) 053001 [`arXiv:1207.2594`] [ɪɴSPIRE].

[64] S. Kashiwase and D. Suematsu, *Leptogenesis and dark matter detection in a TeV scale neutrino mass model with inverted mass hierarchy*, *Eur. Phys. J.* **C 73** (2013) 2484 [`arXiv:1301.2087`] [ɪɴSPIRE].

[65] Planck collaboration, P.A.R. Ade et al., *Planck 2015 results. XIII. Cosmological parameters*, *Astron. Astrophys.* **594** (2016) A13 [`arXiv:1502.01589`] [ɪɴSPIRE].